Physics Journal
Vol. 3, No. 1, 2017, pp. 1-12
http://www.aiscience.org/journal/pj
ISSN: 2471-8483 (Print); ISSN: 2471-8491 (Online)

Phase Lag Elimination at All Frequencies for Full State Estimation of Spacecraft Attitude

Timothy Sands*

Department of Mechanical Engineering, Stanford University, Stanford, USA

Abstract

This research paper describes a development to eliminate phase lag permitting a single commercially available sensor (Global Positioning System, GPS receiver) to provide full-state knowledge (including angular acceleration), eliminating the need for accelerometers, rate gyros, and other sensors. GPS position data is used to provide full-state estimates using high gain observers, and two topologies (Gopinath and Luenberger) are examined and compared, and example preferred design choices are discussed. Observer gain tuning is illustrated and assertions are evaluated via simulations. A major weakness of feedback state observers if phase lag (90 degrees per unit of system order) so in particular, novel methods are introduced to achieve near-zero phase lag state estimation at all frequencies.

Keywords

Topologies, Estimation, Gopinath, Luenberger, Phase Lag, Full State Feedback, GPS

Received: September 19, 2017 / Accepted: November 9, 2017 / Published online: December 9, 2017

1. Introduction

The basic idea is to provide knowledge of a spacecraft's attitude, attitude rate, and angular acceleration using only position measurement via the global positioning systems (GPS) without having exceedingly noisy state estimates. The lofty goal is to replace high cost on-board attitude sensors with low-cost GPS antennae and specialized algorithms. [1]

Table 1. Typical accuracies of objects sensed.

Reference object	Typical accuracies
Stars	1 arc second
Sun	1 arc minute
Earth (horizon)	6 arc minutes
RF beacon	1 arc minute
Magnetic field	30 arc minutes
Global Positioning System	6 arc minutes

Anyone interested in angular state identification would benefit from this development, but in particular the focus remains spacecraft developers and operators. Customers include government agencies (e.g. the National Aeronautics and Space Administration, NASA; the Department of Defense, DoD; the Department of Energy, DoE; etc.), but additionally several commercial companies develop and operate spacecraft for non-governmental purposes (e.g. Lockheed-Martin, Hughes, Orbital Sciences, etc.). Typical attitude knowledge requirements vary for disparate spacecraft missions. The requirements drive the choice of sensor. The sensor choice comes with penalties in weight and power, both of which are premiums for space missions. Some examples of typical design solution choices are listed in Table 1 from [2] and Table 2 from [3].

1.1. Prior Research

NASA Goddard's Navigator team developed a new receiver that allows spacecraft to quickly acquire GPS navigational signals in weak-signal areas. Seeing an opportunity to help lower mission costs, the NASA Navigator team, led by Goddard engineer Luke Winternitz, used Research and

* Corresponding author
E-mail address: dr.timsands@stanford.edu

Development (R&D) funding to develop algorithms and hardware for a prototype spacecraft GPS receiver that would allow spacecraft to acquire and track weak GPS signals at an altitude of 100,000 km (62,137 miles); well above the GPS constellation, roughly one quarter of the distance to the moon. Winternitz and his team from NASA are currently developing the next-generation Navigator receiver; one that can acquire the GPS signal even if the spacecraft carrying the receiver is located at lunar distances. Such a capability would reduce mission operational costs because ground controllers could track spacecraft via GPS rather than with expensive ground stations. [4]

Table 2. Typical system accuracy and characteristics.

Sensor	Accuracy	Characteristics and Applicability
Magnetometers	1^o at 5000km 5^o at 200km	Attitude measured relative to Earth's local magnetic field. Magnetic field uncertainties and variability dominate accuracy. Usable only below ~6000km.
Earth Sensors	0.05^o at GEO 0.1^o at low altitude	Horizon uncertainties dominate accuracy. Highly accurate unites use scanning.
Sun Sensors	0.01^o	Typical field of view $\pm 130^0$
Star Sensors	2 arc sec	Typical field of view $\pm 16^0$
Gyroscopes	0.001 deg/hr	Normal use involves periodically resetting the reference position
Directional Antenna	0.01^o to 0.05^o	Typically 1% of beamwidth

Table 3. Typical hardware component weight and power.

Component	Weight (kg)	Power (W)
Earth Sensor	2 to 3.5	2 to 10
Sun Sensor	0.2 to 1	0 to 0.2
Magnetometer	0.1 to 1.5	0.2 to 1
Gyroscope	0.8 to 3.5	2 to 20
Processors	5 to 25	5 to 25

David Quinn [5] invented a GPS system for navigation and attitude determination, comprising a sensor array including a convex hemispherical mounting structure having a plurality of mounting surfaces, and a plurality of antennas mounted to the mounting surfaces for receiving signals from space vehicles of a GPS constellation. His invention includes a receiver for collecting the signals and making navigation and attitude determinations. There may alternatively be two opposing convex hemispherical mounting structures, each of the mounting structures having a plurality of mounting surfaces, and a plurality of antennas mounted to the mounting surfaces.

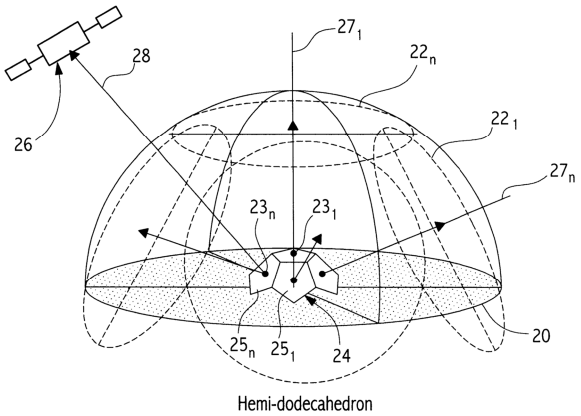

Figure 1. Block diagram of the hemi-dodecahedron antenna array and receiver. [5].

Recently, flight results from the Radio Aurora Explorer (RAX) satellites, RAX-1 and RAX-2, which are CubeSats developed to study space weather, demonstrated a multiplicative extended Kalman filter is used for attitude estimation. On-orbit calibration was developed and applied to compensate for sensor and alignment errors, and attitude determination accuracies of 0.5° 1–σ have been demonstrated on-orbit. It is noteworthy that multiplicative extended Kalman filtering is at the high-end of computational requirements. Simpler approaches are valuable for space missions, where every pound to orbit can be quite expensive. In this paper, simpler estimation approaches will be evaluated, including Gopinath-styled and Luenberger-styled observers.

1.2. Distinctiveness of This Development

NASA Goddard's Innovative Technology Partnerships Office Home currently invites companies to license a new method for low-noise attitude rate determination that uses Global Positioning System (GPS) signals and eliminates the need for heavy and expensive gyroscopes and star trackers [7]. Currently methods use the Doppler differences [8] among GPS signals to calculate highly accurate attitude rates, offering a low-noise, lightweight, and lower cost method for determining attitude rate for satellites and potentially for aviation and marine vehicles.

This development will seek to accomplish similar results (low-noise, lightweight, and lower cost) without using Doppler information. Since gyroscopes and star trackers are extremely expensive, this technology can result in a major reduction in cost and has the potential to significantly reduce weight as well as enable navigation control by a single/few GPS receiver(s).

Current GPS devices estimate attitude rates using a phase-locked loop process, which is very noisy and requires data to go through a low-pass filter in order to be meaningful. This filtering, however, limits high-frequency rates that the system can handle. The goal is to not use the GPS receiver rate

estimates, while obtaining angular position, angular rate, and perhaps angular acceleration with only GPS position and attitude data and simple algorithms (requiring less computation than say Kalman Filtering), and simultaneously reduce noise.

Lastly and perhaps most importantly, observer gain tuning for two topologies will be introduced to achieve near-zero phase lag estimation at all frequencies.

2. Materials and Methods

2.1. Relevant Sensor Technologies

There are reasons for current engineers maintaining classical attitude sensor suites on a spacecraft even when a GPS receiver is added. [6], [10] In this case the classical sensors may be allowed to be of modest quality only, as subsequent fusion of their data with those from the GPS receiver may restore the accuracy of the final estimate again to an acceptable level. Hence, low-cost attitude sensors combined with a low-cost GPS receiver can still satisfy non-trivial attitude reconstitution accuracy requirements. Several different options are available for determining the spacecraft attitude commonly used today. Several examples are listed below. [2]

2.1.1. Magnetometers

In flux gate magnetometer, alternating current is passed through one coil, and a perm alloy core is alternately magnetized by electromagnetic field. The corresponding magnetic field is sensed by second coil. The distortion of the oscillating field is a measure of one component of the Earth's magnetic field. Three magnetometers are required to determine Earth's magnetic field vector.

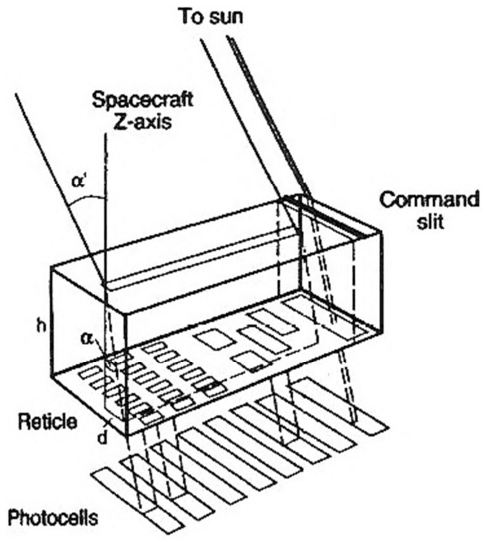

Figure 2. Sun Sensor [2].

2.1.2. Sun Sensors

A transparent block of material with known refractive index, n, is coated with an opaque material (Figure 2). Light passes through a slit etched in the top onto receptive areas etched in bottom. Light from the sun passes through the slit, forming a line over the photodetectors. The distance from the centerline is measured by the sensed pattern, which determines angle. With index of refraction, n, the angle to sun is determined using Snell's Law. Photodetectors may provide digital (coarse) or analog (fine) outputs.

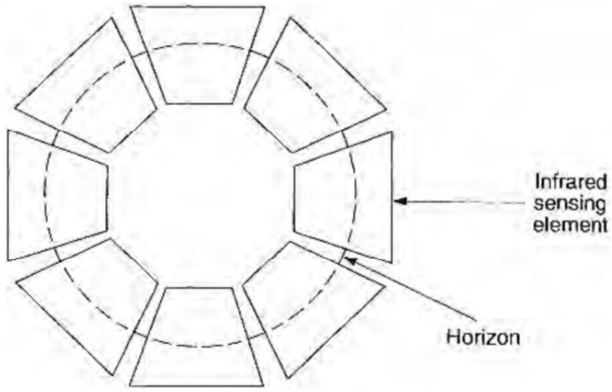

Figure 3. Static Horizon Sensor [2].

2.1.3. Earth's Horizon Sensor

Static horizon sensors typically use infrared sensing to reduce optical error in a manner depicted in Figure 3. The field of view is larger than the entire earth's edge (limb), so the sensor provides orientation with respect to the nadir.

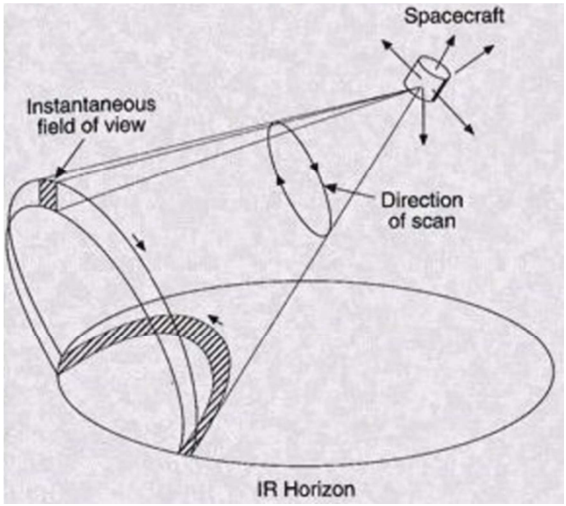

Figure 4. Scanning Horizon Sensor [2].

Scanning horizon sensors use spinning assemblies to identify light and dark areas (of infrared) on the focal array. The width of light area identifies spacecraft roll angle.

2.1.4. Star Sensors

These instruments have narrow fields of view, and must have a low angular velocity to compare stars to a star-location catalog to identify the target. The x and y location of the

star's image on focal plane determines angles to the star. One example is the Goodrich star tracker (Table 4).

Performance Category	Narrow FOV	Wide FOV
Field of View (FOV)	8° X 8°	20° circular
Magnitude Sensitivity	+6.5	+5.1
Power (avg. at +45oC	10W	10W
Weight (with lightshade)	8.5 lb	7.5 lb
Update rate	6 Hz	2 Hz
Simultaneous tracking	6 stars	6 stars
Overall Accuracy		
- Pitch/Yaw, rms	2 arc sec	5 arc sec
- Roll, rms	40 arc sec	40 arc sec

Figure 5. Goodrich star tracker.

2.1.5. Gyroscopes

Mechanical Gyroscopes use the body-axis moment equation (aka "Newton-Euler's Moment equation) to be derived in Section 2.5.1, which turn out to be nonlinear relationships in all three axes.

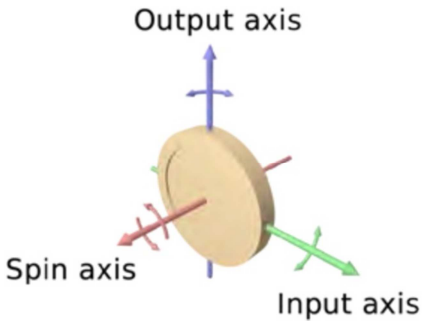

Figure 6. Mechanical gyroscope.

Simplifying assumptions include a constant nominal spin rate about the z-axis with small perturbations in angular velocity about the other two axes. Assuming the moment of inertia about the spin axes is relatively maximal, while the other two moments of inertia are equal to each other also helps. Then linearization produces expressions for perturbations in angular acceleration of the input and output axes. This motivates me to later seek a development that also can produce angular acceleration (in addition to position and rate) to eliminate any justification for needing the gyroscope, which is relatively expensive and also prone to mechanical failure.

Two-degree-of-freedom gyroscopes place a free gyroscope on a gimbaled platform. The gyro essentially "stores" reference directions in space, and then angle pickoffs on the gimbal axes measure pitch and yaw angles.

Large angle feedback may be used with gyroscopes to produce a rate gyro, analogous to a mechanical spring constraint, while large angle rate feedback may be used to produce an integrating gyro, analogous to a mechanical damper restraint.

Optical gyros use Sagnac interferometry to measure rotational rate. When no rotation is present, photons traveling in opposite directions complete the circuit (Figure 7) in the same time. When a rotational rate is present, travel lengths and times are different, and a simple equation relates the time of arrival of light to the rotational rates that are present.

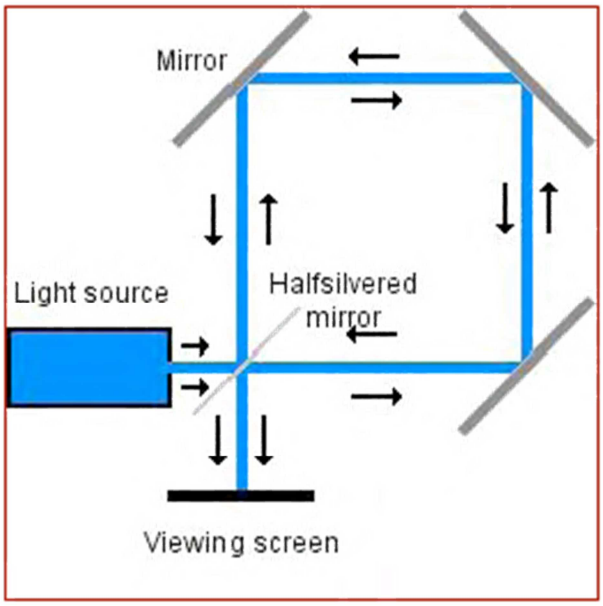

Figure 7. Optical gyroscope.

2.2. Global Positioning Systems [3], [4]

The Global Positioning System (GPS) is a U.S.-owned spacecraft constellation that provides users with positioning, navigation, and timing (PNT) services. This system consists of three segments: the space segment, the control segment, and the user segment. The U.S. Air Force develops, maintains, and operates the space and control segments.

GPS positioning works on two basic mathematical concepts. The first is called trilateration, which literally means positioning from three distances. The second concept is the relationship between distance traveled, rate (speed) of travel and amount of time spent traveling, or:

$$\text{Distance} = \text{Rate} \times \text{Time} \quad (1)$$

The first concept, trilateration, is the focus here. It centers around finding your position on the Earth by knowing the location of orbiting GPS satellites and the distance from those satellites to your location on the planet. However, there is no way to actually take a yardstick, tape measure, etc., and measure the distance from your location up to the satellites. The trick lies in the fact that GPS satellites are always sending out radio signals.

In GPS positioning the rate is how fast the radio signal travels, which is equal to the speed of light (299,792,458

meters per second). Time is determined by how long it takes for a signal to travel from the GPS satellite to a GPS receiver on earth. With a known rate and a known time we can solve for the distance between satellite and receiver. Once we have the distance from at least 3 satellites, we can determine a 3 dimensional position on or above the surface of the earth.

This development will utilize this position measurement and relate it to the angle measurement via rigid body dynamics, and then expand to angular velocity, and angular acceleration utilizing classical state observers. Alternatively, the attitude output of the GPS receiver [5] may be directly fed into the state observers. This later approach was critically evaluated in simulation and frequency response analysis in the next section.

2.3. Details of This Development

Equation of motion and observer tuning are provided next, and later implemented in MATLAB/SIMULINK which is depicted at the end of the article in Figure 20.

2.3.1. Equations of Motion [9]

Notice by using the definition of angular momentum in a body frame, we can reveal a rigid-body spacecraft's angular velocity by knowing the position-rate of a point on the rigid body and knowing the fixed relationship of that point to the body's center of mass.

$$H_B = \lim_{N\to\infty} \sum_{i=1}^{N} \left[\underline{\rho}_B^i \times \left(\Delta m_i \underline{\dot{r}}_i\right)\right] \quad (2)$$

$$H_B = \int_M \left(\underline{\rho}_B \times \underline{V}\right) dm \quad (3)$$

V is the velocity of dm

$\underline{V}_B$ is the velocity of the body

Taking the limit as N→ ∞ in our calculations of the system of *particles* the resultant external torque with respect to B: $\dot{H}_B + \underline{V}_B \times \underline{P} = M_B$. If $\underline{M}_B = 0$ and $\underline{V}_B = 0$ or B is the CM or $\underline{V}_B \parallel \underline{V}_C$ then $\underline{H}_B$ is constant, and thus, *Conservation of Angular Momentum*.

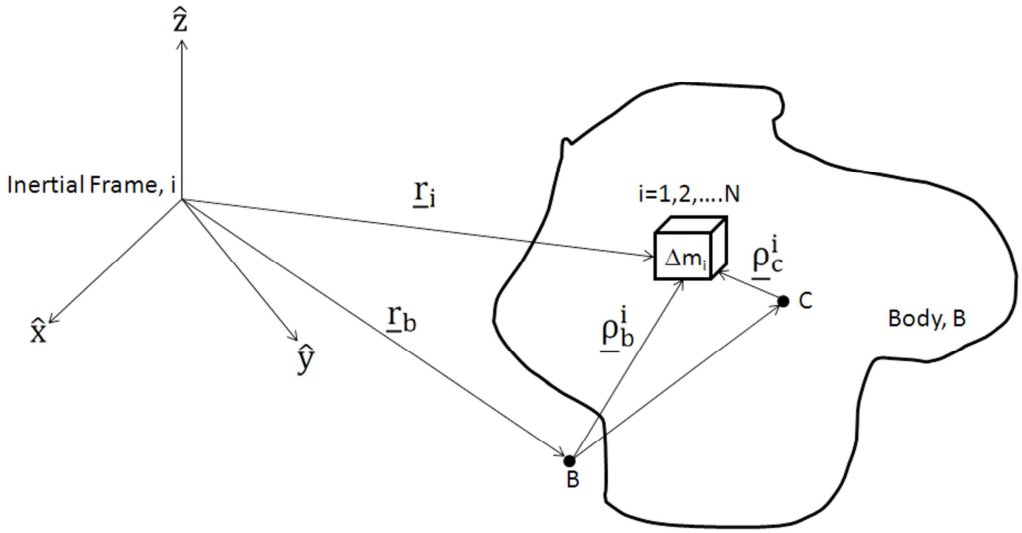

Figure 8. Rigid-body spacecraft.

Another form of the angular momentum principle is in [9] equation 18.22: $\underline{M}_B = \dot{\underline{H}}_B + \underline{\omega} \times \underline{H}_B$ proves to be a much more useful form and bestows one relationship between velocity through linear momentum and angular velocity through angular momentum. By defining the centroidal moment of inertia, we reveal the body's angular velocity.

$$\underline{H_C} = \int_M \left(\underline{\rho_C} \times \underline{\omega} \times \underline{\rho_C}\right) dm \quad (4)$$

$$\underline{H_C} = \int_M \left(\underline{a} \times \underline{b} \times \underline{c}\right) dm \quad (5)$$

$$\underline{H_C} = \int_M \left[(\underline{a} \cdot \underline{c})\underline{b} - (\underline{a} \cdot \underline{b})\underline{c}\right] dm \quad (6)$$

$$\underline{H_C} = \int_M \left[\underbrace{\left(\underline{\rho_C} \cdot \underline{\rho_C}\right)\underline{\omega}}_{(1)} - \underbrace{(\underline{\rho_C} \cdot \underline{\omega})\underline{\rho_C}}_{(2)}\right] dm \quad (7)$$

where $\underline{a} \cdot \underline{b} = \sum_{i=1}^{n} (a_i b_i)$

After a few math steps, we arrive at

$$\underline{H_C} = \int_M \begin{bmatrix} {y_C}^2 + {z_C}^2 & -x_C y_C & -x_C z_C \\ -x_C y_C & {x_C}^2 + {z_C}^2 & -y_C z_C \\ -x_C z_C & -y_C z_C & {x_C}^2 + {y_C}^2 \end{bmatrix} \begin{Bmatrix} \omega_x \\ \omega_y \\ \omega_z \end{Bmatrix} dm \quad (8)$$

Then, defining the centroidal moment of inertia:

$$[I_C] \equiv \int_M \begin{bmatrix} {y_C}^2 + {z_C}^2 & -x_C y_C & -x_C z_C \\ -x_C y_C & {x_C}^2 + {z_C}^2 & -y_C z_C \\ -x_C z_C & -y_C z_C & {x_C}^2 + {y_C}^2 \end{bmatrix} dm \quad (9)$$

Resulting by substitution in the following:

$$\underline{H_C} = [I_C]\{\underline{\omega}\} \quad (10)$$

The rotational motion law is often referred to as Newton-Euler, and it may be paraphrased as: "the summed torque vector [3x1] acting on a body is proportional to its resultant angular acceleration vector [3x1], and the constant of proportionality is the body's mass inertia matrix [3x3]." Newton-Euler also only applies in a non-moving, inertial frame. The equations needed to express the spacecraft's rotational motion are valid relative to the inertial frame (indicated by subscript "B/i" often assumed) and may be expressed in inertia. The motion measurement relative to the inertial frame is taken from onboard sensors expressed in a body fixed frame.

$$\dot{\vec{H}} = \left\{\frac{d\vec{H}}{dt}\right\}_i = \left\{\frac{d\vec{H}}{dt}\right\}_B + \{\vec{\omega}\}^{B/i} \times \{\vec{H}\}_B \text{where } \{\vec{H}\}_B = [J] \cdot \{\vec{\omega}\}^{B/i} \quad (11)$$

$$\sum\{\vec{T}\}_{B/i} \rightarrow \{\tau\}_B = \{\dot{H}\} = [J]\{\dot{\omega}\} + \{\omega\} \times [J]\{\omega\} \quad (12)$$

With proper initialization, the angular velocity can be integrated to provide angular position, but should not be differentiated to seek angular acceleration. Differentiation is inherently a noisy process and numerically differentiating noisy-measurements amplifies the noise, and thus angular acceleration obtained this way would be garbage. Other methods are used including various forms of Kalman Filtering and a simpler approach, state observers. Two kinds of state observers are evaluated here, both high gain observers: Gopinath-styled observers and Luenberger-styled observers per [14].

2.3.2. Equations of State Estimation

Luenberger-styled observers (henceforth simply referred to as Luenberger observers) are a simple method to estimate velocity given position measurements. Additionally, the Luenberger observer may be used to provide estimates of external system disturbances, since the observer mimics order of actual systems dynamic equations of motion. When used the Luenberger disturbance observer bestows robustness to system parameter variations, which will be evaluated shortly.

2.3.3. Observer Gain Tuning

For desired observer eigenvalues λ_1=12.5, λ_2=50, λ_3=200, desired motion controller gains (tuned for disturbance rejection) λ_{c1}=6, λ_{c2}=25, λ_{c3}=100, and current regulator gain λ_i=800, the general form of the characteristic equation may be equated to the specific observer forms, controller form and current regulator form revealing gains [20]-[22]. Tuning was identical for the two observer topologies to permit apples-to-apples comparison (Figure 20) of effects on estimation accuracy. *Observer robustness is assessed by implementing error in the known inertia matrix*. Thus, the known inertia matrix [J] will be different than the estimated inertia matrix $[\hat{J}]$.

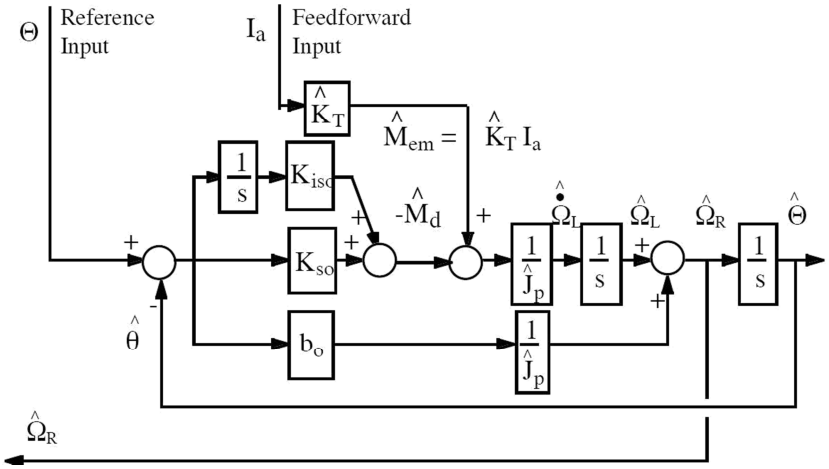

Figure 9. Luenberger-Styled Observer.

2.3.4. Luenberger Tuning (Actual Current)

This method uses the actual current from the spacecraft actuator circuit (rather than modeled or predicted current) to provide the feedforward element of the observer. The actuator circuit is assumed to be a DC brushless motor actuating a momentum exchange device (e.g. reaction wheel, control moment gyroscope, etc.). In a DC brushless motor, the armature is fixed, while permanent magnets rotate, while an electronic controller commutates the electromagnetic force providing a rotating field.

Figure 10. DC Brushless motor [2].

This position would normally include the actual current or control, u in typical observer designs (recalling that observer design is a dual process of controller design). Utilizing the reference input and actual circuit moment, you can produce an estimate of remaining disturbance (normally fed back to feedback controllers to handle).

$$C.E.= (s+\lambda_1)(s+\lambda_2)(s+\lambda_3) = \hat{J}_p s^3 + b_o s^2 s + K_{so} s + K_{iso} \quad (13)$$

$$b_o = \hat{J}_p(\lambda_1+ \lambda_2+ \lambda_3) \quad (14)$$

$$K_{so} =\hat{J}_p([\lambda_1(\lambda_2+ \lambda_3)+ \lambda_2 \lambda_3] \; K_{iso} = \hat{J}_p(\lambda_1 \lambda_2 \lambda_3) \quad (15)$$

Gopinath Tuning:

$$\frac{\hat{\omega}(s)}{\omega(s)} = \frac{(K_{T1}s^2+K_{T2}s+K_{T3})\left(\frac{J_p s^2(L_p-\hat{L}_p)+J_p(R_p-\hat{R}_p)s}{K_T}+\frac{\hat{K}_t}{K_t}J_p s(\hat{L}_p+\hat{R}_p)\right)}{\hat{J}_p\hat{L}_p s^3+(J_p R_p+\hat{K}_e K_1)s^2+\hat{K}_e K_2 s+\hat{K}_e K_3} \quad (14)$$

Equating coefficient of 's' and solve for gains:

$$(s+\lambda_1)(s+\lambda_2)(s+\lambda_3)= \hat{J}_p s^3 + (\hat{J}_p\hat{R}_p+\hat{K}_e K_1)s^2 + \hat{K}_e K_2 s + \hat{K}_e K_3 \quad (17)$$

$$K_{T1} = \frac{\hat{J}_p\hat{L}_p(\lambda_1+ \lambda_2+ \lambda_3)-\hat{J}_p\hat{R}_p}{\hat{K}_e} \quad (15)$$

$$K_{T3} = \frac{\hat{J}_p\hat{L}_p}{\hat{K}_e}\left(\lambda_1\lambda_2\lambda_3\right) \quad (16)$$

$$K_{T2} = \frac{\hat{J}_p\hat{L}_p(\lambda_1 \lambda_2+ \lambda_3)-\hat{J}_p R_p\left(\lambda_1(\lambda_2+ \lambda_3)+ \lambda_2 \lambda_3\right)}{\hat{K}_e} \quad (17)$$

Motion Controller used for simulation comparison:

$$(s+\lambda_{c1})(s+\lambda_{c2})(s+\lambda_{c3}) =\hat{J}_p s^3 + b_a s^2 s + K_s s + K_{is} \quad (18)$$

$$\text{Current regulator: } (s+\lambda_i) = L_p s+R_a \quad (19)$$

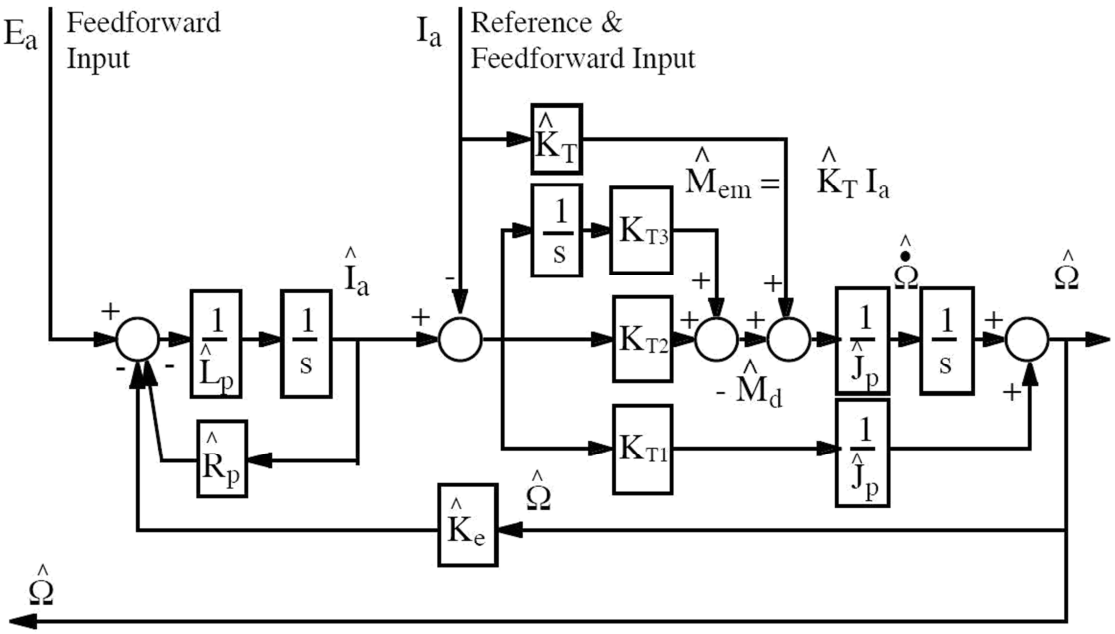

Figure 11. Gopinath-Styled Velocity Observer.

Observer estimation frequency response functions were calculated and plotted first for ±20% estimated-inertia error then for the case of ±20% error in estimate of K_e=K_t (Figure & Figure 2). Notice first that for all cases of zero-error, both observers exactly estimate the angular velocity of motion. Overall, the Gopinath-styled observer (referred to as simply "Gopinath" for brevity) performed poorer than the Luenberger-styled observer indicating the Luenberger observer is less parameter-sensitive with respect to inertia, K_e, and K_t.

While the Luenberger observers diverge very close to the maximum tuned bandwidth (even with parameter errors), the Gopinath observer diverges at a lower bandwidth when errors are present. Since both observers contain a current-feedforward element, you will see nearly zero-lag properties out to the bandwidth of the feedback observer controller. Clearly, disturbances (in the form of modeling errors here) do not influence low frequency estimation (likely due to the addition of integrators in the observer controllers).

The Gopinath observer was particularly sensitive to errors in K_t indicating its reliance on the feedforward estimation path. Notice in particular in Figure & Figure 2 that zero-lag estimation occurs even with inaccurate K_t (albeit with non-zero estimation frequency response at all frequencies).

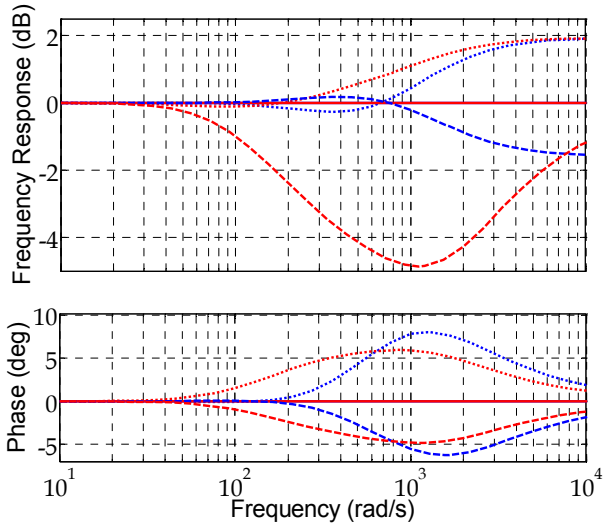

Figure 12. Estimation accuracy for incorrect $\hat{J}_p$.

Figure 12 displays a comparison of estimation accuracy frequency response functions for incorrect $\hat{J}_p$. Luenberger (blue) Gopinath (red); dotted = -20% error, solid = 0% error; dashed = +20% error. Figure 13 displays Comparison of estimation accuracy frequency response functions for incorrect Kt=Ke. Luenberger (blue) Gopinath (red); dotted = -20% error, solid = 0% error; dashed = +20% error.

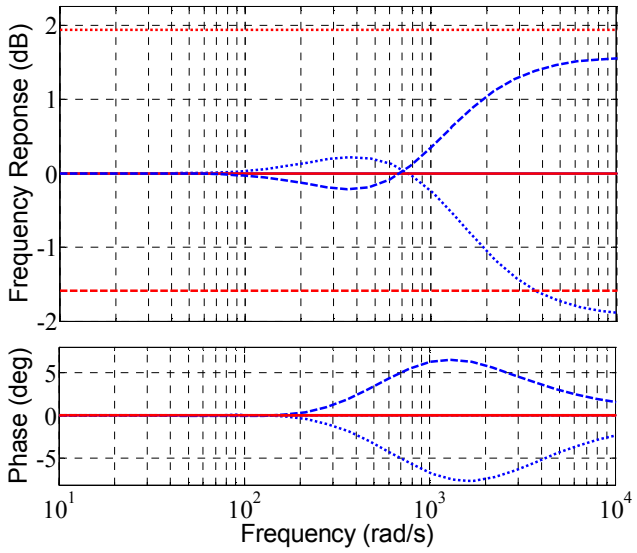

Figure 2. Estimation accuracy for incorrect Kt=Ke.

Table 4. Observer Gains.

Luenberger Gains		
b_o	K_{so}	K_{iso}
Nm/m/s	Nm/m	Nms
24.74	7772.3	465090
Gopinath Gains		
KT1	KT2	KT3
rad/s Nms /A	Nm/A	Nms/A
0.4813	238.7	14285

2.3.5. Angular Rate Estimation Using Only Position

Time-response simulations were run with identically tuned observers with a sample commanded trajectory (rotation angle) of θ*(t)=sin(10t). Iterations were run to establish the effects of 20% inertia underestimation and the effects of sensor noise on command tracking accuracy. Sensor noise was modeled as random numbers with zero-mean and unity variance.

Figure 20 displays the methodology for apples-to-apples comparison of effects on command tracking. Manual switches were used to evaluate a given case with the results displayed in Figure 3 and Figure 4.

General conclusions may be drawn. Nominal feedback control handles incorrect-estimation just fine from the perspective of control, but not knowledge. This is especially since inertia has nothing to do with the feedback control strategy (lacking a feedforward strategy). Using the Luenberger observer performs nearly as well if actual attitude angle θ(t) is used for estimation, while it does not perform as well when θ*(t) (commanded angle) is used for estimation. This is intuitive, since θ*(t) does not include the errors and noises associate with the process, while θ(t) includes these errors and noises. In all cases examined, the Gopinath observer was inferior to Luenberger observers, which reinforces the earlier revelation of parameter sensitivity (in the discussion of the estimation frequency response functions). In addition to examining the effects on command tracking accuracy, estimation accuracy was plotted from the simulations to confirm the indications garnered from the discussion of Figure & Figure 2 (estimation accuracy frequency response functions, FRFs). The single case of 20% inertia underestimation with zero-mean and unity variance sensor noise confirmed that the Luenberger observer provided superior estimates compared to the Gopinath observer for this sinusoidal commanded trajectory.

Figure 14 displays the Frequency Response Functions (FRF) for the motion control system. The red-solid line is tracking function, and blue dotted line is disturbance response. Figure 15 Estimation errors for $\hat{J}_p$ = 0.8Jp and μ=0, λ^2=1 sensor noise. Black solid line is Luenberger with θ(s) input; Green dotted line is Luenberger with θ*(s) input; red solid line is Gopinath with Ia(s) input; blue dotted line is Gopinath with I*(s) input.

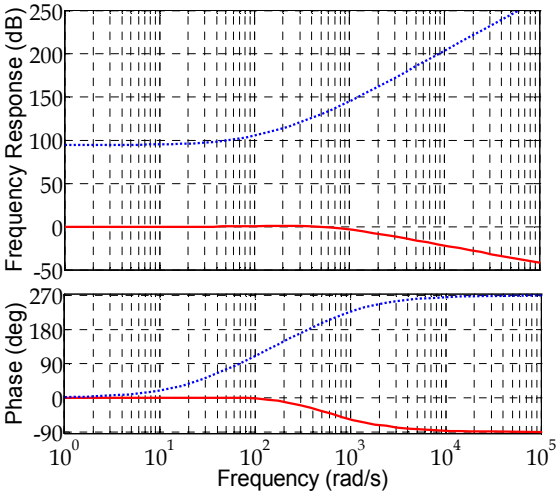

Figure 3. Motion Control Frequency Response Functions.

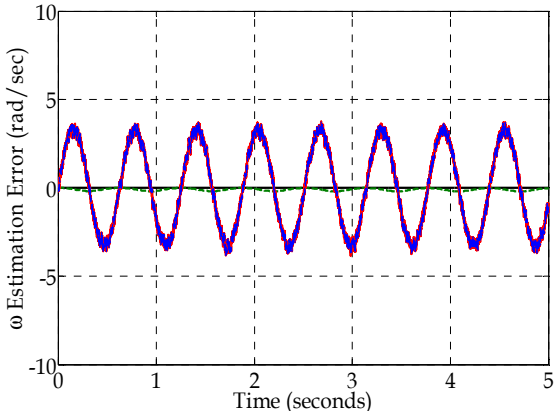

Figure 4. Estimation errors for $\hat{J}_p = 0.8Jp$ and $\mu=0$, $\lambda^2=1$ sensor noise.

2.4. Summary of Observers' Utility

We see that classical state observers can effectively produce estimates of angular acceleration using a procedure that uses proportional-integral estimation (thus noise-smoothing). Then the estimates are integrated once and twice for estimates of angular rate and position respectively after adding a derivative component to estimation. Frequency response evaluation demonstrated near-zero lag estimation of the full-state using only position & angle data from a GPS sensor.

3. Results – a Preferred Design

Following from the preceding development, the favored design approach is to use a commercial space-rated GPS receiver with onboard avionics executing a Luenberger observer to produce angular acceleration estimates via proportional-integral estimation. This estimate is integrated (smoothing noise) and derivative-action is added to the estimation of angular velocity. The angular velocity estimated is integrated (further smoothing noise) to produce angle estimates with demonstrated high-accuracy.

3.1. Sensors

GPS receivers have been produced on chips making them rapidly useful for spacecraft applications. [13] Specific GPS receivers may be chosen to meet pointing requirements, electrical compatibility, and other performance specifications. The SGR-05U [18], GPS-12-VA [18] and Namuru, for example have very low (~1W) power requirements, while TOPSTAR 3000D [16] has more performance history (e.g. Demeter, Swift Gamma-Ray Burst Missions, etc.).

Table 5. Observer Gains.

Receiver	Accuracy	Cost
SGR-05U	10m LEO 1cm/s LEO	$25,900
Namuru V2 or 3	2cm LEO	$6,600
TOPSTAR 3000	10m LEO 100m GEO	$13,624 recurring $13624 non-recurring
GPS-12-VA	10m LEO 0.03 m/sec LEO	$25,900

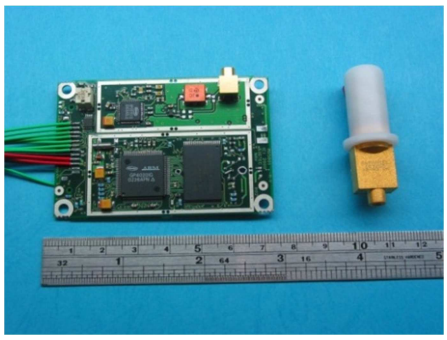

Figure 16. SGR-05U GPS receiver.

3.2. Interface Specifications

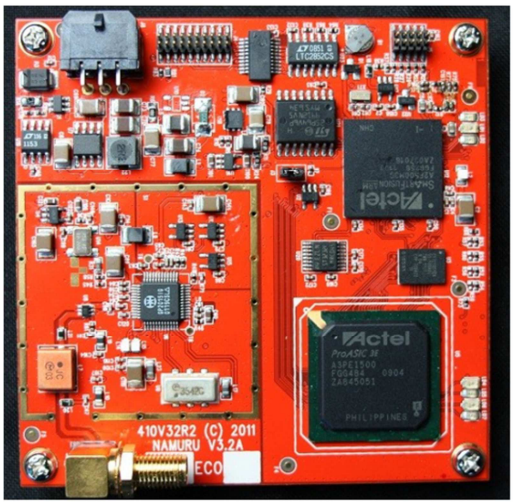

Figure 5. Namuru V3.2 GPS receiver.

One example interface specification is taken from the AMS-02 spaceflight experiment using the TOPSTAR 3000 [16]. Interface hardware includes merely the STR4500 Spirnet

communications cable for wireless antenna, the receiver, and PC Windows! The only software necessary for that mission was the SimpLEX software package, due to the International Space Station already having the SPRIRENT software system. I recommend utilizing MATLAB/SIMULINK with XPC Target or other such operating systems for easy implementation of various observers in the single operating software if possible; otherwise implement the observers in the software system of choice by the space mission. MIL-STD 1553 is the standard for the bus. "Space qualified" receivers comply with ISO9001 and AQAP110. Sample functional architecture and receiver diagrams are included in Figure 18 and Figure 19.

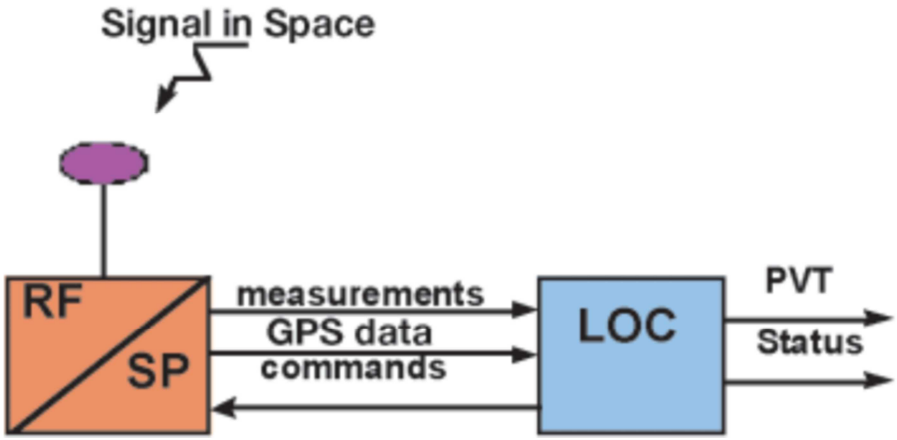

Figure 18. Functional architecture [14].

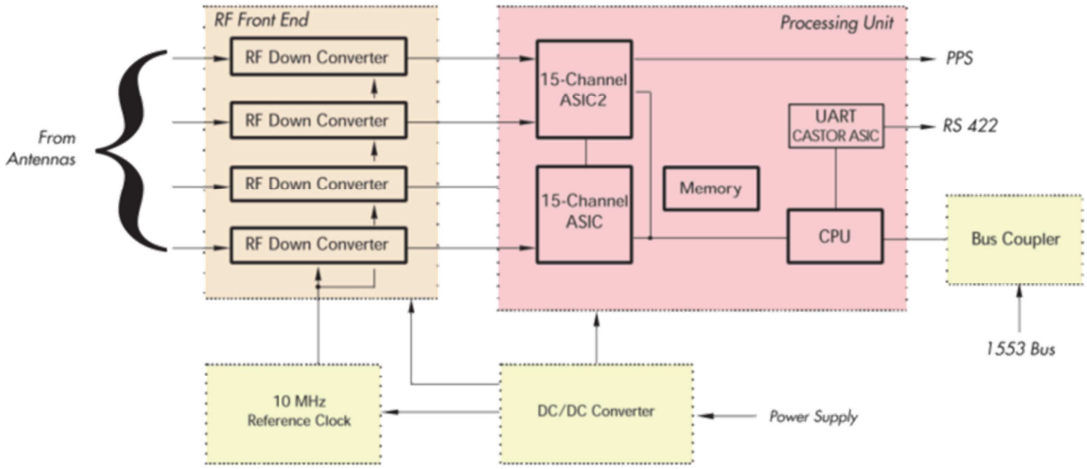

Figure 19. Receiver Diagram [16].

3.3. Estimation of Electronics Complexity and Costs

Complexity will be low, while costs will vary by choice of hardware and software to meet mission requirements (some exterior to mere knowledge requirements, e.g. mission requirements). GPS receivers have become mature for space-use, and furthermore classical state observers are ubiquitously known. The prototype observers are already built, and the receivers are commercially available. To implement this development, simply feed the GPS position signal into avionics program implementing the estimated full-state in motion controllers expecting good results as presented here.

4. Discussion

The basic idea is to provide knowledge of attitude, attitude rate, and angular acceleration using only position measurement via the global positioning systems (GPS) without having exceedingly noisy state estimates. The lofty goal is to replace high cost on-board attitude sensors with low-cost GPS antennae and specialized algorithms. Not only have Luenberger and Gopinath estimator topologies achieved the objective, enhancing the topologies with feedforward elements [15], [20]-[27] yields *near-zero phase lag* estimation at all frequencies. In light of the impacts of phase lag, it may be asserted this novel approach should be considered the new initial baseline standard to begin design

of state estimators, and future research should begin from this new baseline seeking further improvements, including optimization for various cost functions.

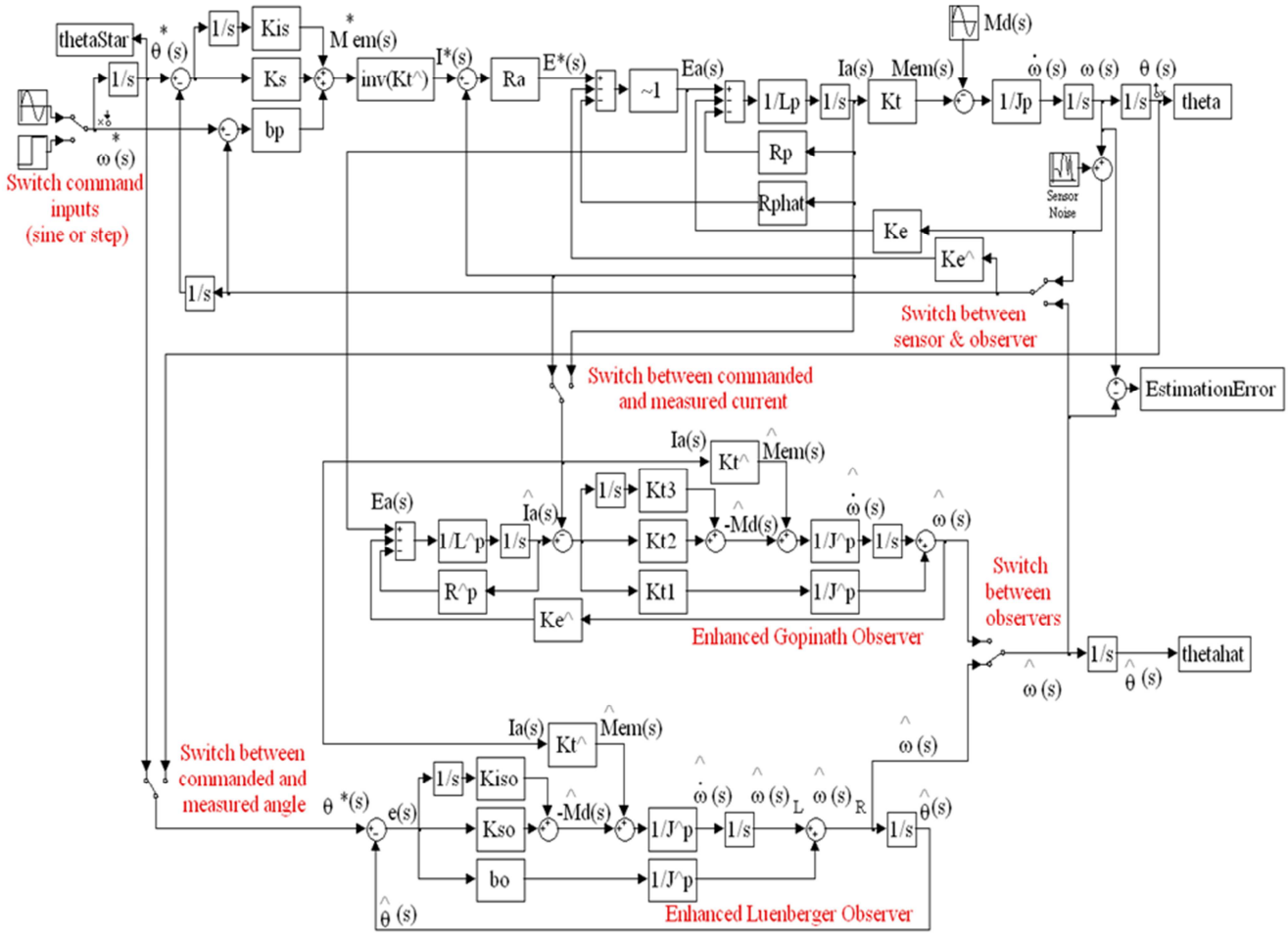

Figure 20. SIMULINK model for error comparison.

References

[1] GPS. GOV website: Official Government information about the global positioning system: http://www.gps.gov/applications/space/

[2] R. Stengel coursenotes, MAE342 Space System Design, Princeton University; available at http://www.princeton.edu/~stengel/MAE342Lecture13.pdf.

[3] Larson, Wertz, Space Mission Analysis and Design, Third Ed., Microcosm Press, El Segundo, 1999.

[4] http://www.nasa.gov/topics/technology/features/navigator-gps.html

[5] Quinn, David A. 2003. GPS compound eye attitude and navigation sensor and method. U.S. Patent 6594582 B1, filed May 12, 2000, and issued Jul 15, 2003.

[6] Crassidis, J. L., and Lightsey E. G., "Attitude Determination Using Combined GPS and Three-Axis Magnetometer Data," Space Technology, Vol. 22, No. 4, 2001, pp. 147-156.

[7] http://www.acsu.buffalo.edu/~johnc/gps.htm

[8] NASA Goddard Innovative Technology Partnerships Office homepage: http://techtransfer.gsfc.nasa.gov/ft_tech_gps_doppler.shtm

[9] Campbell; Charles E., 2003. Using the global positioning satellite system to determine attitude rates using doppler effects. U.S. Patent 6,593,879, filed August 9, 2001, and issued July 15, 2003.

[10] Beer, Johnston, Mazurek, Cornwell, Eisenberg, Vector Mechanics for Engineers 9th Edition, McGraw-Hill, 2010.

[11] Q. P. Chu, P. Van Woerkom, "GPS for low-cost attitude determination: A review of concepts, in-flight experiences, and current developments", Acta Astronautica, Volume 41, Issues 4–10, August–November 1997, Pages 421–433.

[12] Lightsey, E. G., Ketchum, E., Flatley, T. W., Crassidis, J. L., Freesland, D., Reiss, K., and Young, D., "Flight Results of GPS Based Attitude Control on the REX II Spacecraft," ION-GPS-96, Kansas City, MO, Sept. 1996, pp. 1037-1046.

[13] J. C. Springmann, J. W. Cutler, "Flight results of a low-cost attitude determination system", Acta Astronautica, Volume 99, June–July 2014, Pages 201–214.

[14] C. Duncan, "GPS On A Chip" -- An Advanced GPS Receiver for Spacecraft, NASA research paper, 1998. Available at: http://trs-new.jpl.nasa.gov/dspace/bitstream/2014/20504/1/98-1493.pdf

[15] Sands, T., "Physics-Based Control Methods," book chapter in Advancements in Spacecraft Systems and Orbit Determination, edited by Rushi Ghadawala, Rijeka: In-Tech Publishers, pp. 29-54, 2012.

[16] T. Mekky A. Habib, “Combined spacecraft orbit and attitude control through extended Kalman filtering of magnetometer, gyro, and GPS measurements”, The Egyptian Journal of Remote Sensing and Space Science, 20 January 2014.

[17] www.esa.int/esapub/bulletin/.../gerner104.pdf

[18] Surrey Satellite Technology US, LLC catalog: http://www.sst-us.com/shop/satellite-subsystems/gps/sgr-05u-space-gps-receiver

[19] Spacequest catalog: http://www.spacequest.com/products/GPS-12-V1.pdf

[20] T. Sands, “Fine Pointing of Military Spacecraft”, Ph.D. Dissertation, Naval Postgraduate School, Monterey, CA, USA, 2007.

[21] T. Sands, R. Lorenz, "Physics-Based Automated Control of Spacecraft" AIAA Space 2009, AIAA #167790, 2009.

[22] S. Nakatani, T. Sands, “Simulation of Spacecraft Damage Tolerance and Adaptive Controls” *Proceedings of IEEE Aerospace*, Big Sky, MT, USA, 1–8 March 2014.

[23] Sands, T., "Improved Magnetic Levitation via Online Disturbance Decoupling", Physics Journal, Vol. 1, No. 3, Oct. 19, 2015

[24] S. Nakatani, T. Sands, “Autonomous Damage Recovery in Space”, *International Journal of Automation, Control and Intelligent Systems*, 2(31), 2016.

[25] P. Heidlauf, M. Cooper, “Nonlinear Lyapunov Control Improved by an Extended Least Squares Adaptive Feed forward Controller and Enhanced Luenberger Observer”, *Proceedings of the International Conference and Exhibition on Mechanical & Aerospace Engineering*, Las Vegas, NV, USA, 2–4 October 2017.

[26] M. Cooper, P. Heidlauf, T. Sands, “Controlling Chaos—Forced van der Pol Equation”, *Mathematics*, 5(70), 2017.

[27] T. Sands, “Nonlinear-Adaptive Mathematical System Identification”, *Computation*, submitted to special issue - Computational Engineering, Dec 2017 - Jan 2018.